K_2 can be expressed in terms of $z_{\min}$ as

$$K_2 = 1 - e^{-\frac{E_b}{N_o}\frac{1}{N_r}z_{\min}} \cdot e^{-\frac{E_b}{N_o}\frac{1}{N_r}(2-2^m)}. \quad (33)$$

Hence, the ratio between K_1 and K_2 can be expressed and simplified as

$$\frac{K_1}{K_2} = \frac{1}{e^{\frac{E_b}{N_o}\frac{1}{N_r}(2^m-1)}\left[e^{(\epsilon_m 2^{m-2}-1)}-1\right]}.$$

As (34), shown below, implies, K_1/K_2 becomes much smaller when $m \geq 2$ and E_b/N_0 is in the medium-to-high-SNR range. Consequently, we have

$$\sum_{k\neq 1}\binom{2k}{k}\frac{1}{N}\left\{\frac{e^{-\frac{E_b}{N_o}\frac{k}{N_r}(2+2z_{\min})}}{\left[1-e^{-\frac{E_b}{N_o}\frac{1}{N_r}\epsilon_m 2^{m-2}}\right]^{2k}}\right\} \approx 0. \quad (34)$$

■

REFERENCES

[1] S. Imada and T. Ohtsuki, "Prerake diversity combining for UWB systems in IEEE 802.15 UWB multipath channel," in *Proc. IWUWBS*, May 2004, pp. 236–240.

[2] T. Strohmer, M. Emami, J. Hansen, G. Papanicolaous, and A. J. Paulraj, "Application of time-reversal with MMSE equalization to UWB communications," in *Proc. IEEE GLOBECOM*, Nov. 2004, vol. 5, pp. 3123–3127.

[3] Y.-H. Chang, S.-H. Tsai, X. Yu, and C.-C. J. Kuo, "Design and analysis of channel-phase-precoded ultra wideband (CPPUWB) systems," in *Proc. IEEE WCNC*, Apr. 2006, pp. 866–871.

[4] M. Z. Win and R. A. Scholtz, "On the energy capture of ultrawide bandwidth signals in dense multipath environments," *IEEE Commun. Lett.*, vol. 2, no. 9, pp. 245–247, Sep. 1998.

[5] P. Komulainen and K. Pehkonen, "A low complexity superorthogonal turbo-code for CDMA applications," in *Proc. IEEE PIMRC*, Taipei, Taiwan, Feb. 1996, vol. 2, pp. 369–373.

[6] *Channel Modelling Sub-Committee, Final Report*, Feb. 2003. IEEE 802.15.SG3a, IEEE P802.15-02/490r1-SG3.

[7] A. Saleh and R. Valenzuela, "A statistical model for indoor multipath propagation," *IEEE J. Sel. Areas Commun.*, vol. SAC-5, no. 2, pp. 128–137, Feb. 1987.

[8] A. Rajeswaran, V. S. Somayazulu, and J. R. Foerster, "RAKE performance for a pulse based UWB system in a realistic UWB indoor channel," in *Proc. ICC*, May 2003, vol. 4, pp. 2879–2883.

[9] U. Riaz, M.-O. Pun, and C.-C. J. Kuo, "Performance analysis of ultra-wide band impulse radio (UWB-IR) with super-orthogonal turbo codes (SOTC)," in *Proc. IEEE Globecom*, San Francisco, CA, Nov. 2006, pp. 981–985.

[10] P. Komulainen and K. Pehkonen, "Performance evaluation of super-orthogonal turbo codes in AWGN and flat Rayleigh fading channels," *IEEE J. Sel. Areas Commun.*, vol. 16, no. 2, pp. 196–205, Feb. 1998.

[11] D. Divsalar, "A simple tight bound on error probability of block codes with application to turbo codes," Jet Propuls. Lab., California Inst. Technol., Pasadena, CA, pp. 42–139, TMO Progress Rep. 42-139, Nov. 1999.

[12] D. Divsalar, S. Dolinar, and F. Pollara, "Iterative turbo decoder analysis based on density evolution," *IEEE J. Sel. Areas Commun.*, vol. 19, no. 5, pp. 891–907, May 2001.

EXIT-Chart-Aided Three-Stage Concatenated Ultrawideband Time-Hopping Spread-Spectrum Impulse Radio Design

R. A. Riaz, R. G. Maunder, M. F. U. Butt, S. X. Ng, S. Chen, and L. Hanzo

***Abstract*—A serially concatenated and iteratively decoded Irregular Variable-Length Coding (IrVLC) scheme is amalgamated with a unity-rate precoded time-hopping (TH) pulse-position-modulation (PPM)-aided ultrawideband (UWB) spread-spectrum (SS) impulse radio design. The proposed design is capable of operating at low SNRs in Nakagami-m fading channels contaminated by partial band noise jamming (PBNJ) as a benefit of lossless IrVLC joint source and channel coding. Although this scheme may readily be used for lossless video or audio compression, for example, we only used it here for lossless near-capacity data transmission. A number of component variable-length-coding (VLC) codebooks having different coding rates are utilized by the IrVLC scheme for encoding specific fractions of the input source symbol stream. EXtrinsic Information Transfer (EXIT) charts are used to appropriately select these fractions to shape the inverted EXIT curve of the IrVLC and, hence, to match that of the inner decoder, which allows us to achieve an infinitesimally low bit error ratio (BER) at near-capacity SNR values.**

***Index Terms*—EXIT charts, impulse radio, irregular code design, spread-spectrum communications, three-stage concatenated iterative detection, time-hopping, ultrawideband, ultrawideband systems, unity-rate codes, variable-length codes.**

I. INTRODUCTION

The novel contribution of this paper is that we advance the design of time-hopping pulse-position-modulation ultrawideband (TH-PPM-UWB) systems with the aid of sophisticated channel coding in the interest of approaching attainable capacity. More specifically, our TH-PPM-UWB design exploits that, analogous to irregular convolutional coding [1], the family of Irregular Variable-Length Codes (IrVLCs) [2] employs a number of component variable-length-coding (VLC) codebooks having different coding rates [3] for encoding particular fractions of the input source symbol stream. The appropriate lengths of these fractions may be chosen with the aid of EXtrinsic Information Transfer (EXIT) charts [4] to shape the inverted EXIT curve of the IrVLC codec to ensure that it does not cross the EXIT curve of the inner channel codec. This way, an open EXIT chart tunnel may be created even at near-capacity values of SNR.

UWB communications systems are commonly defined as systems that have either more than 20% relative bandwidth compared with the band's center frequency or more than 500-MHz absolute bandwidth. The pioneering work of Win and Scholtz [5]

Manuscript received June 15, 2009; revised June 23, 2009. First published June 23, 2009; current version published November 11, 2009. This work was supported by the Engineering and Physical Sciences Research Council, U.K., under the EU Optimix project.

R. A. Riaz and M. F. U. Butt are with the School of Electronics and Computer Science, University of Southampton, SO17 1BJ Southampton, U.K., and also with the Department of Electrical Engineering, COMSATS Institute of Information Technology, Islamabad 44000, Pakistan (e-mail: rar06r@ecs.soton.ac.uk; mfub06r@ecs.soton.ac.uk).

R. G. Maunder, S. X. Ng, S. Chen, and L. Hanzo are with the School of Engineering and Computer Science, University of Southampton, SO17 1BJ Southampton, U.K. (e-mail: rm@ecs.soton.ac.uk; sxn@ecs.soton.ac.uk; sqc@ecs.soton.ac.uk; lh@ecs.soton.ac.uk).

Digital Object Identifier 10.1109/TVT.2009.2025857

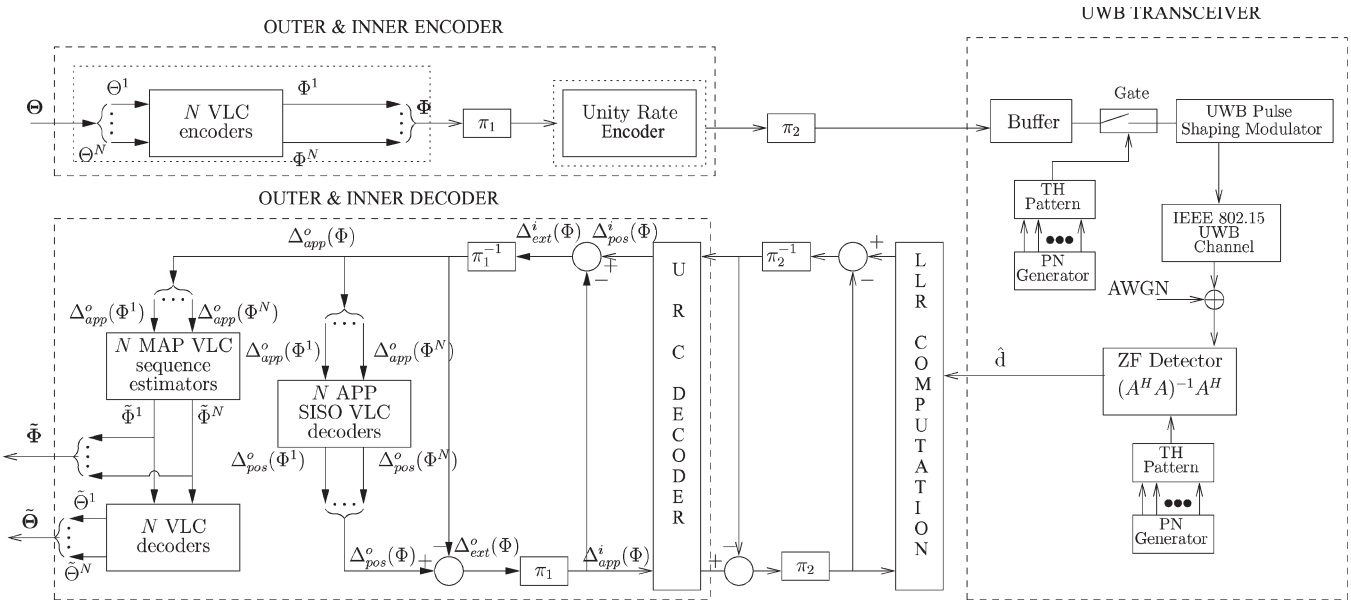

Fig. 1. Schematic of the IrVLC- and VLC-based TH-PPM-UWB schemes. In the IrVLC-coded scheme, we have $N = 16$, whereas in the VLC-coded scheme, $N = 1$.

developed the concept of TH-PPM-UWB impulse radio systems. In the aforementioned systems, trains of time-shifted PPM pulses are used to transmit baseband or carrierless UWB signals.

Against this background, as a further contribution of this paper, we extend the concept of classic two-stage extrinsic information (EI) exchange [6] to a three-stage UWB scheme constituted by a unity-rate decoder, an IrVLC decoder, and the TH-PPM-UWB detector. Although this scheme may readily be used for lossless video or audio compression, for example, we only used it here for lossless near-capacity data transmission. The technique of EXIT charts is utilized to investigate the serial concatenation of the TH-PPM-UWB detector, the unity-rate decoder, and the IrVLC outer decoder to attain good performance, even at near-capacity SNR values. We demonstrate that the three-stage scheme outperforms the two-stage benchmarker. The practical rationale of the proposed system is that of achieving lossless video or data file transmission in emerging high-rate universal-serial-bus-type applications, for example. Finally, a further novel aspect worthy of mention is that the system imposes transmission efficiency by further compressing the source data.

This paper is organized as follows: In Section II, our complete system design philosophy is elaborated. In Section III, our EXIT chart and bit error ratio (BER) results are discussed as a function of the IrVLC code parameters. Finally, in Section IV, we present our conclusions.

II. System Overview

A. System Description

Our design considered in Fig. 1 assumes 16-ary VLC source symbol values obeying a 16-ary discrete probability density function (pdf) resulting from the Lloyd–Max (LM) quantization of independent Laplacian-distributed source samples. The dynamic range of the symbol probabilities lies between 0.002 and 0.16 when considering 4-bit LM quantization. The entropy of the 16 symbols obeying these probabilities lies between 2.6 and 8.74 bits/symbol with an overall source entropy of 3.5 bits per VLC symbol. The rationale of the proposed IrVLC coding scheme is that, given this nonuniform probability of occurrence for the 16 VLC symbols and their associated entropies, the VLC scheme is capable of data compression and high-integrity detection at near-capacity SNRs.

The transmitter shown in Fig. 1 transmits the source symbol frame $\mathbf{\Theta}$, which comprises J number of source symbols having $K = 16$-ary values $\{\Theta_j\}_{j=1}^{J} \in [1, \ldots, K]$. These source symbols are decomposed into N number of components $\{\mathbf{\Theta}^n\}_{n=1}^{N}$, where we opted for $N = 16$ in the case of the IrVLC-TH-PPM-UWB scheme considered and $N = 1$ in the case of the regular VLC-based benchmarker scheme. The number of symbols in the source symbol frame $\mathbf{\Theta}$, which is decomposed into the source symbol frame component $\mathbf{\Theta^n}$, is specified as J^n, where we have $J^1 = J$ in the case of the VLC-based scheme. By contrast, in the case of the IrVLC-based scheme, the specific values of $\{J^n\}_{n=1}^{N}$ may appropriately be chosen to shape the inverted EXIT curve of the IrVLC codec so that it does not cross the EXIT curve of the precoder, as detailed in [7].

Each of the N source symbol frame components $\{\mathbf{\Theta}^n\}_{n=1}^{N}$ is VLC encoded using the corresponding codebook from the set of N VLC codebooks $\{\mathbf{VLC}^n\}_{n=1}^{N}$ having a range of coding rates $\{R^n\}_{n=1}^{N} \in [0, 1]$. The specific source symbols having the value of $k \in [1, \ldots, K]$ and encoded by the specific VLC codebook $\mathbf{VLC}^n$ are represented by the codeword $\mathbf{VLC}^{n,k}$, which has a length of $I^{n,k}$ bits. The J^n number of VLC codewords that represent the J^n number of source symbols in the source symbol frame component $\mathbf{\Theta^n}$ are concatenated to provide the transmission frame component $\mathbf{\Phi^n} = \{\mathbf{VLC}^{n,\Theta_{j^n}^n}\}_{j^n=1}^{J^n}$.

Depending on the specific length of the VLC codewords, the number of bits comprised by each transmission frame component $\mathbf{\Phi^n}$ will typically slightly vary from frame to frame. To facilitate the VLC decoding of each transmission frame component $\mathbf{\Phi^n}$, it is necessary to explicitly convey its length $I^n = \sum_{j^n=1}^{J^n} I^{n,s_{j^n}^n}$ to the receiver with the aid of side information. The N transmission frame components $\{\mathbf{\Phi}^n\}_{n=1}^{N}$ encoded by the different IrVLC component codes are concatenated at the transmitter, as shown in Fig. 1. The resultant transmission frame $\mathbf{\Phi}$ has a length of $\sum_{n=1}^{N} I^n$ bits. Following the bit interleaver π_1, the transmission frame $\mathbf{\Phi}$ is precoded and then interleaved again by the bit interleaver π_2. The interleaved bits are sent to the buffer depicted in Fig. 1. These bits are transmitted by the TH-PPM modulator.

B. UWB Transmission and Detection

TH-PPM-UWB: A general TH-PPM-UWB signal is given by

$$g(t) = \sum_{n=-\infty}^{\infty} \phi(t - nT_F - T_{\mathrm{PP}_n} - T_{\mathrm{CH}_n}) \tag{1}$$

where $\phi(t)$ is the signaling pulse shape, T_F is the frame duration, T_{PP_n} is the PPM-related shift in the pulse position, either forward or backward with respect to the nominal signaling instant to represent the binary stream, and T_{CH_n} is the time shift based on the unique user-specific TH code reminiscent of the pseudonoise sequence of a specific user, where the code repeats after a certain interval. The frame duration T_F is typically on the order of 1000 times the actual pulsewidth to avoid any intersymbol interference imposed by multipath propagation.

Channel Model: The channel impulse response (CIR) ratified by the IEEE 802.15.3 standard and considered here can be expressed as [8]

$$h(t) = \sum_{l=1}^{L} h_l e^{j\varphi_l} \delta(t - lT_\varphi) \tag{2}$$

where L represents the number of resolvable paths, whereas h_l and φ_l are the gain and the phase of the lth resolvable CIR tap. Furthermore, lT_φ represents the corresponding delay of the lth CIR tap. As shown in [9] and [10], the CIR taps of the UWB channel follow Nakagami distribution, which has been validated by using Kolmogorov–Smirnov testing at a significance level of 1%. We assume in our analysis that the phase rotation imposed by the channel is uniformly distributed in $[0, 2\pi]$. The transmitted signal is also corrupted by both additive white Gaussian noise and partial band noise jamming (PBNJ) having single-sided power spectral densities of N_0 and N_J, respectively.

ZFD: The data estimates $\hat{\mathbf{d}}$ at the output of the zero-forcing detector (ZFD) are

$$\hat{\mathbf{d}}_{\mathrm{ZFD}}|_{\mathbf{R}_n=\sigma^2 I} = (\mathbf{A}^{\mathbf{H}}\mathbf{A})^{-1}\mathbf{A}^{\mathbf{H}}\mathbf{y} \tag{3}$$

where $\mathbf{n}$ is the noise sequence, which has a covariance matrix of $\mathbf{R}_n = E[nn^H]$, and $\mathbf{A}$ is the overall system matrix. Equation (3) assumes that $\mathbf{n}$ consists of noise samples that are zero-mean Gaussian variables having a variance of σ^2 with the corresponding covariance matrix $\mathbf{R}_n = \sigma^2 I$, where I is the identity matrix [11]. After the ZFD, the corresponding symbol probabilities and log-likelihood ratios (LLRs) are computed, which are then fed to the unity-rate decoder in Fig. 1.

C. Iterative Decoding

The conditional probability of the jth transmitted symbol Θ_j, where $j = 0, \ldots, J-1$, given the signal $\hat{\mathbf{d}} = [d_0, d_1, \ldots, d_{J-1}]$, which represents the set of J outputs of the ZFD in Fig. 1, is given by

$$P(\Theta_j|\hat{\mathbf{d}}) = \frac{p(\hat{\mathbf{d}}|\Theta_j)P(\Theta_j)}{p(\hat{\mathbf{d}})} \tag{4}$$

where $p(\hat{\mathbf{d}}|\Theta_j)$ is the pdf of the received signal $\hat{\mathbf{d}}$ given that Θ_j is transmitted. Furthermore, $P(\Theta_j)$ is the *a priori* probability of the symbol Θ_j, whereas $p(\hat{\mathbf{d}}) = \sum_{j=0}^{J-1} p(\hat{\mathbf{d}}|\Theta_j)P(\Theta_j)$ is the probability of receiving the signal set $\hat{\mathbf{d}}$. At the first iteration, we have $P(\Theta_j) = 1/J$ for all the transmitted symbols, since no *a priori* information is available. The pdf $p(\hat{\mathbf{d}}|\Theta_j)$ uniquely determines the statistics required for estimating the probability $P(\Theta_j|\hat{\mathbf{d}})$. The expression of $p(\hat{\mathbf{d}}|\Theta_j)$ is given by

$$p(\hat{\mathbf{d}}|\Theta_j) = f_{d_j}(v_j|\Theta_j) \prod_{x=0, x\neq j}^{J-1} f_{d_n}(v_x|\Theta_j) \tag{5}$$

where $f_{d_n}(v_x|\Theta_j)$ represents the pdf of the xth detector value, $x = 0, 1, \ldots, J-1$, given that Θ_j is transmitted. The simplified expression for $p(\hat{\mathbf{d}}|\Theta_j)$ is

$$p(\hat{\mathbf{d}}|\Theta_j) = \exp\left(\frac{v_j\gamma_h}{1+\gamma_h}\right) \tag{6}$$

where $\gamma_h = bRE_b/(N_0L)$ is the SNR per hop, R is the code rate, E_b is the transmitted energy per bit, and $b = \log_2 M$ is the number of bits per symbol. The corresponding LLRs [4] can be computed from (5) and (6).

The derivation of the soft information from the received signal is different for the two- and three-stage serial concatenated schemes. In the first case, the unity-rate *a posteriori probability* (APP) soft-input–soft-output (SISO) decoder and the outer decoder exchange EI to perform iterative detection (ID), both invoking the Bahl–Cocke–Jelinek–Raviv algorithm using bit-based trellises. Again, we refer to this ID-aided configuration as the *two-stage scheme*. Alternatively, the system may be modified so that the TH-PPM-UWB detector, the unity-rate inner decoder, and the IrVLC outer decoder exchange their EI, as shown in Fig. 1. We refer to this arrangement as the *three-stage scheme*. The three-stage scheme requires the additional interleaver π_2 between the precoder and the TH-PPM-UWB detector in Fig. 1.

Since N separate VLC encoders are employed in the TH-PPM-UWB transmitter, N separate VLC decoders have to be used in the corresponding receiver seen in Fig. 1. In parallel with the composition of the bit-based transmission frame $\mathbf{\Phi}$ from N VLC source symbols, the *a priori* LLRs $\Delta^o_{\mathrm{app}}(\mathbf{\Phi})$ are decomposed into N components, as shown in Fig. 1, although each of the components processes a proportionely reduced number of symbols. Hence, the associated complexity is only modestly increased. This is achieved with the aid of the explicit side information that we assume to be available for conveying the slightly varying number of bits I^n of each transmission frame component $\mathbf{\Phi^n}$. Each of the N VLC decoders is provided with the *a priori* LLR subframe $\Delta^o_{\mathrm{app}}(\mathbf{\Phi^n})$, and in response, it generates the *a posteriori* LLR subframe $\Delta^o_{\mathrm{pos}}(\mathbf{\Phi^n})$, $n \in [1, \ldots, N]$. These *a posteriori* LLR subframes are concatenated to provide the *a posteriori* LLR frame $\Delta^o_{\mathrm{pos}}(\mathbf{\Phi})$.

During the final decoding iteration, N bit-based maximum APP VLC sequence estimation processes are invoked instead of single-class APP SISO VLC decoding, as shown in Fig. 1. In this case, each transmission frame component $\mathbf{\Phi^n}$ is estimated from the corresponding *a priori* LLR frame component $\Delta^o_{\mathrm{app}}(\mathbf{\Phi^n})$. The resultant transmission frame component estimates $\tilde{\mathbf{\Phi}}^{\mathbf{n}}$ may be concatenated to provide the transmission frame estimate $\tilde{\mathbf{\Phi}}$. Additionally, the transmission frame component estimates $\tilde{\mathbf{\Phi}}^{\mathbf{n}}$ may be VLC decoded to provide the source symbol frame component estimates $\tilde{\mathbf{\Theta}}^{\mathbf{n}}$.

III. Performance Analysis

We have used $N = 16$-component VLC codebooks $\{\mathbf{VLC}^n\}_{n=1}^N$ having approximately equally spaced coding rates in the range of [0.2, 0.95] in the TH-PPM-UWB scheme. Moreover, unless otherwise stated, we employ the following parameter values: source symbol frame length of $J = 80\,000$, outer code rate of $R = 0.5$, TH-PPM-UWB spreading factor of $M = 16$, and a diversity order of $L = 3$. In each case, we employ a variable-length error-correcting codebook [3] that is tailored to the source symbol values' probabilities of

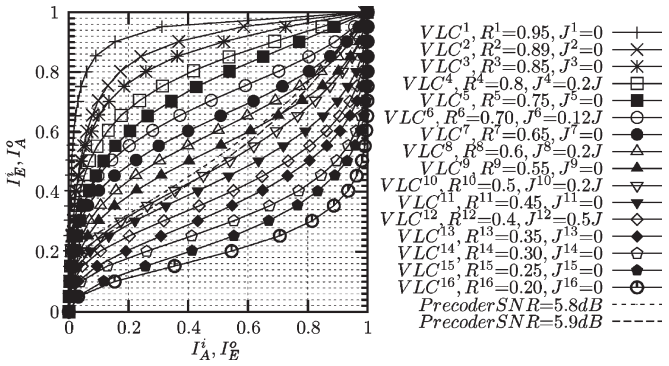

Fig. 2. Inverted VLC EXIT curves and unity-rate decoder EXIT curves, assuming uncorrelated Nakagami-m fading channel.

occurrence. Again, these codes compress the unequal probability input data symbols for the sake of achieving a near-entropy source rate and a lower probability at near-capacity SNRs. By contrast, in the VLC benchmarker scheme, we employ just $N = 1$ VLC codebook, which is identical to the VLC codebook $\mathbf{VLC}^{10}$ of the IrVLC scheme having a coding rate of $R = 0.5$. Note that this coding rate results in an average interleaver length of $J \cdot E/R$ bits. The inverted EXIT curve of the IrVLC scheme is also shown in Fig. 2, assuming an uncorrelated Nakagami-m fading channel contaminated by PBNJ characterized by $E_b/N_J = 10$ dB and a jamming factor of $\rho = 0.1$. This was obtained as the appropriately weighted superposition of the $N = 16$ component VLC codebooks' inverted EXIT curves, where the weight applied to the inverted EXIT curve of the component VLC codebook $\boldsymbol{VLC}^{\mathbf{n}}$ is proportional to the specific number of source symbols employed for encoding J^n [1]. Using the approach in [1], the values of $\{J^n\}_{n=1}^N$ given in Fig. 2 were designed so that the IrVLC composite coding rate matches that of our regular VLC benchmarker scheme, namely, 0.5. Furthermore, we ensured that the inverted IrVLC EXIT curve did not cross the unity-rate decoder's EXIT curve at E_b/N_0 of 5.9 dB. We note that only four out of the 16 VLC components were indeed activated by the algorithm in [1] to encode a nonzero number of source symbols. As shown in Fig. 2, the presence of an open EXIT chart tunnel implies that an infinitesimally low BER may be achieved by the TH-PPM-UWB scheme for E_b/N_0 values above 5.9 dB. By contrast, an open EXIT chart tunnel is not afforded for E_b/N_0 values below 5.8 dB in the case of the VLC-based benchmarker scheme.

Analogous to the IrVLC design in Fig. 2, we have also designed IrVLC codes for both two- and three-stage ID-aided schemes, assuming various jamming scenarios in Nakagami-m fading channels. The design parameter values are listed in Table I, where the relevant minimum values of $E_b/N_0(dB)$ or $E_b/N_J(dB)$ at which an open convergence tunnel is formed are shown alongside the specific fractions of the source symbol frame encoded by each component code of the IrVLC scheme given by $\alpha_n = J^n/J$. Both the EXIT-chart-based and the Monte Carlo simulation-based convergence SNR values are shown in Table I for both IrVLC and VLC schemes. Here, the theoretical values imply those predicted by the EXIT chart analysis, whereas the actual values are those achieved in the symbol-by-symbol Monte Carlo simulations. The code rates of the IrVLC's component codes used in our simulations are [0.95, 0.89, 0.85, 0.8, 0.75, 0.7, 0.65, 0.6, 0.55, 0.5, 0.45, 0.4, 0.35, 0.3, 0.25, 0.2].

Fig. 3 provides the BER performance of both two- and three-stage schemes versus E_b/N_J, assuming $E_b/N_0 = 10$ dB and $\rho = 0.5$. It becomes explicit from Fig. 3 that the three-stage scheme yields an improvement of nearly 3 dB over the two-stage IrVLC. The performance gain achieved by the three-stage scheme is at the expense of a slightly higher complexity, which is imposed by the extra interleaver and

TABLE I
PARAMETER VALUES FOR THE IRVLC-BASED CONCATENATED SCHEMES

Channel	S	Convergence Min. Value				$\alpha_n = \frac{J^n}{J}$ values
		IrVLC		VLC		
		The.	Act.	The.	Act.	
Interf. free	2	5.7	5.7	5.9	5.9	[0,0,0,0.18,0,0.12,0, 0.18,0,0,0,0.52,0,0,0,0]
	3	4.7	4.8	5.0	5.1	[0,0,0,0.26,0,0.24,0,0, 0,0,0,0.34,0.13,0.03,0,0]
$\frac{E_b}{N_J}$=10 ρ=0.1	2	6.6	6.7	6.9	7	[0,0,0,0.24,0,0,0,0.22, 0,0.03,0,0.5,0,0,0,0]
	3	5.8	5.9	6.1	6.2	[0,0,0,0,0.18,0,0.27,0,0, 0,0,0,0.55,0,0,0,0]
$\frac{E_b}{N_J}$=10 $\rho = 0.5$	2	9.4	10.4	9.8	10.7	[0,0,0,0.08,0,0.16,0.11, 0,0,0.5,0,0,0,0,0,0]
	3	6.8	7.5	7.9	8.7	[0,0,0,0.13,0,0.32,0,0, 0,0,0,0.55,0,0,0,0]

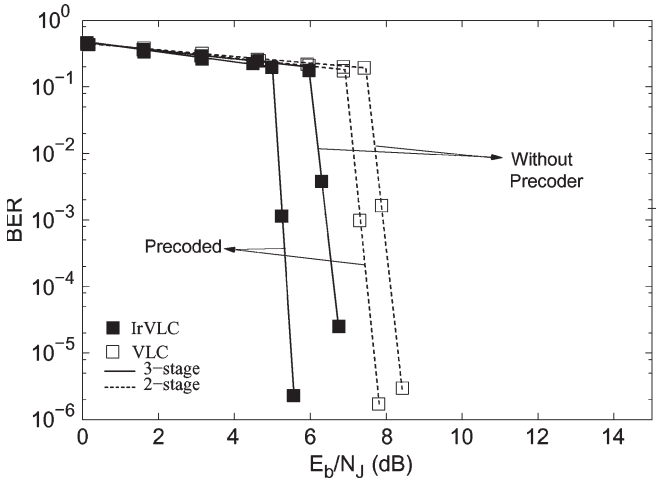

Fig. 3. BER versus E_b/N_J performance of the two- and three-stage VLC- and IrVLC-based schemes in jammed uncorrelated Nakagami-m fading channels assuming $E_b/N_o = 10$ dB and $\rho = 0.5$.

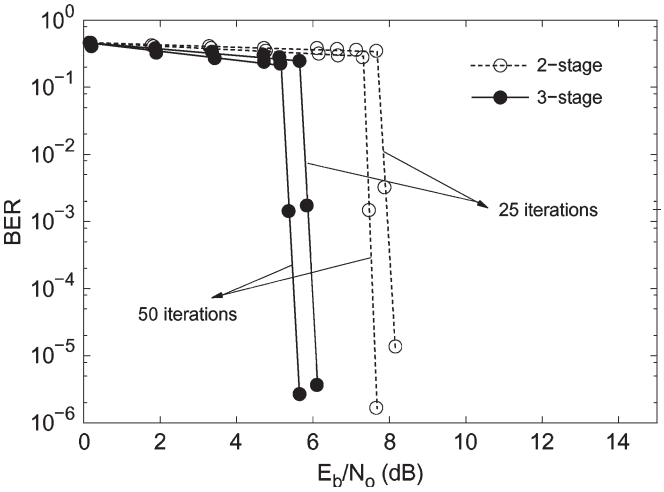

Fig. 4. BER versus E_b/N_o performance of the two- and three-stage VLC- and IrVLC-based schemes in jammed uncorrelated Nakagami-m fading channels, assuming $E_b/N_J = 10$ dB and $\rho = 0.1$.

decoder. Fig. 3 demonstrates that the three-stage scheme outperforms the corresponding VLC-based arrangement by 1.1 dB. The effect of reducing the number of iterations in both two- and three-stage schemes is characterized in Fig. 4. Finally, Fig. 5 portrays the EXIT curves of the IrVLC and unity-rate decoders and the corresponding decoding

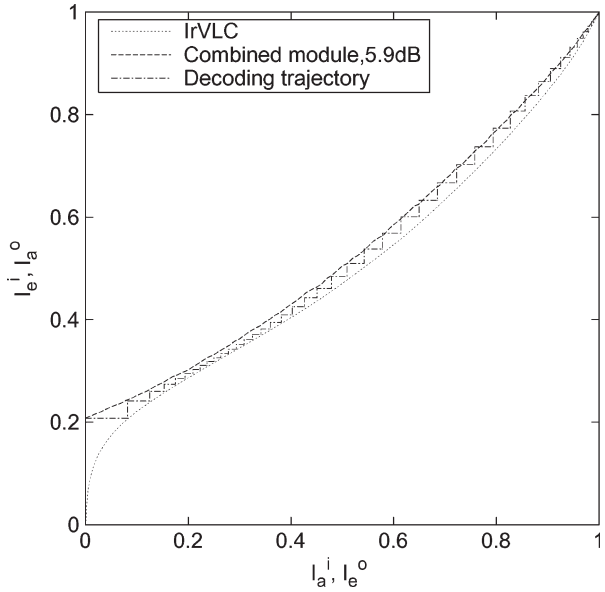

Fig. 5. IrVLC and unity-rate decoder EXIT curves and decoding trajectory assuming jammed uncorrelated Nakagami-m fading channels with $\rho = 0.1$.

trajectory, assuming an interference-free uncorrelated Nakagami-m fading channel for an SNR of 5.9 dB.

IV. Conclusion

In this paper, we have investigated the serial concatenation of IrVLC coding with a TH-PPM-UWB design operating in Nakagami-m fading channel in conjunction with PBNJ. Consequently, we noted that the precoder-aided scheme yields a gain of more than 6.9 dB over the system operating without a precoder. An open EXIT chart tunnel may be created at low SNR values. Moreover, the proposed three-stage design performs 2.9 dB better than the corresponding two-stage scheme.

References

[1] M. Tüchler and J. Hagenauer, "EXIT charts of irregular codes," in *Proc. Conf. Inf. Sci. Syst.,* Princeton, NJ, Mar. 2002, pp. 748–753.

[2] R. G. Maunder, J. Wang, S. X. Ng, L. L. Yang, and L. Hanzo, "On the performance and complexity of irregular variable length codes for near-capacity joint source and channel coding," *IEEE Trans. Wireless Commun.*, vol. 7, no. 4, pp. 1338–1347, Apr. 2008.

[3] V. Buttigieg and P. G. Farrell, "Variable-length error-correcting codes," *Proc. Inst. Elect. Eng.—Commun.*, vol. 147, no. 4, pp. 211–215, Aug. 2000.

[4] S. ten Brink, "Convergence of iterative decoding," *IEEE Trans. Commun.*, vol. 49, no. 10, pp. 1727–1737, Oct. 2001.

[5] M. Z. Win and R. A. Scholtz, "Impulse radio: How it works," *IEEE Commun. Lett.*, vol. 2, no. 2, pp. 36–38, Feb. 1998.

[6] C. Berrou, A. Glavieux, and P. Thitimajshima, "Near Shannon limit error correcting coding and decoding: Turbo codes," in *Proc. IEEE Int. Conf. Commun.*, 1993, pp. 1064–1070.

[7] L. Hanzo, P. Cherriman, and J. Streit, *Video Compression and Communications: From Basics to H.261, H.263, H.264, MPEG4 for DVB and HSDPA-Style Adaptive Turbo-Transceivers*. U.K.: Wiley, 2007.

[8] H. Sato and T. Ohtsuki, "Frequency domain channel estimation and equalisation for direct sequence ultra wideband (DS-UWB) system," *Proc. Inst. Elect. Eng.—Commun.*, vol. 153, no. 1, pp. 93–98, Feb. 2006.

[9] A. F. Molisch, "Ultrawideband propagation channels—Theory, measurement, and modeling," *IEEE Trans. Veh. Technol.*, vol. 54, no. 5, pp. 1528–1545, Sep. 2005.

[10] R. A. Riaz, M. F. U. Butt, S. Chen, and L. Hanzo, "Generic z-domain discrete-time transfer function estimation for ultra-wideband systems," *Electron. Lett.*, vol. 44, no. 25, pp. 1491–1492, Dec. 2008.

[11] L. Hanzo, L.-L. Yang, E.-L. Kuan, and K. Yen, *Single- and Multi-Carrier DS-CDMA: Multi-User Detection, Space–Time Spreading, Synchronisation, Networking and Standards*. New York: Wiley, 2003.

On Power-Loading Algorithms for Packet-Access OFDM Systems

Lin Tang, Honglin Hu, *Member, IEEE*, and Hsiao-Hwa Chen, *Senior Member, IEEE*

***Abstract*—Numerous power-loading techniques for wireless applications have been proposed in the literature. However, most of the existing power-loading schemes may not always be suitable for packet-access orthogonal frequency-division multiplexing (OFDM) systems. In this paper, we propose a Lagrange multiplier power-loading (LMPL) algorithm for packet-access OFDM systems with fixed modulation and coding transmission. The proposed LMPL algorithm offers a closed-form solution for the power-loading optimization problem under a total transmit power constraint. As a closed-form solution may not be available for adaptive modulation and coding (AMC) transmission, we use a low-complexity joint LMPL algorithm to enhance the system throughput. Numerical results show that the proposed LMPL algorithms outperform the traditional channel inversion power-loading (CIPL) scheme. It is also shown that the theoretically derived throughput very well matches the simulation results.**

***Index Terms*—Lagrange multiplier, modulation and coding, orthogonal frequency-division multiplexing (OFDM), power loading, throughput.**

I. Introduction

In frequency-selective fading channels, different orthogonal frequency-division multiplexing (OFDM) subcarriers may experience different channel attenuations. To maximize system throughput, bit/power-loading algorithms are widely used to adaptively adjust power and data rate across the subcarriers in response to varying channel state information (CSI). The optimal solution is to use a water-filling approach [1], where the throughput curve is assumed to approach the Shannon limit, and the power loading is carried out by Lagrange multiplier optimization. However, because the number of different ways for bit assignments is constrained to be an integer in any practical communication system, i.e., the constellation size of modulation and coding schemes (MCSs) is finite, the water-filling-type power loading has to be modified before it can effectively be used.

Numerous power-loading algorithms were proposed to solve the discrete power-loading problem. These algorithms can mainly be classified into two categories: 1) rate-maximization and 2) margin-maximization algorithms. In the rate-maximization algorithms [2]–[6], the total rate of the system is maximized under a total transmit power constraint, whereas in the margin-maximization algorithms [6]–[9], the total transmit power is minimized to meet the total rate constraint. However, all of these bit/power-loading methods were derived for an uncoded OFDM system, meaning that only adaptive modulation is employed. In fact, channel coding is always integrated with different

Manuscript received June 25, 2008; revised January 23, 2009 and April 28, 2009. First published July 7, 2009; current version published November 11, 2009. This work was supported in part by the project of the Science and Technology Commission of Shanghai Municipality under Grant 08511500500 and in part by the Taiwan National Science Council under Grant NSC97-2219-E-006-004. The review of this paper was coordinated by Prof. W. Su.

L. Tang and H. Hu are with the Shanghai Research Center for Wireless Communications, Shanghai 200335, China, and also with the Shanghai Institute of Microsystem and Information Technology, Chinese Academy of Science, Shanghai 200050, China (e-mail: lin.tang@shrcwc.org; hlhu@ieee.org).

H.-H. Chen is with the Department of Engineering Science, National Cheng Kung University, Tainan 701, Taiwan (e-mail: hshwchen@ieee.org).

Color versions of one or more of the figures in this paper are available online at http://ieeexplore.ieee.org.

Digital Object Identifier 10.1109/TVT.2009.2026757